Science Bulletin 71 (2026) 3875–3880

Contents lists available at ScienceDirect

Science Bulletin

journal homepage: www.elsevier.com/locate/scib

Article

Thresholdless corner vortex solitons in fractal Sierpiński topological insulators

Yiqi Zhang [a,*], Alexander V. Kireev [b,c], Victor O. Kompanets [b], Sergey Y. Alyatkin [d], Nikita S. Kostyuchenko [b,e], Sergei A. Zhuravitskii [b,e], Nikolay N. Skryabin [e], Khalil Sabour [c], Alexander A. Kalinkin [e], Yongdong Li [a], Sergei P. Kulik [b,e], Pavlos G. Lagoudakis [d], Sergey V. Chekalin [b], Yaroslav V. Kartashov [b,*], Victor N. Zadkov [b,f]

[a] Key Laboratory for Physical Electronics and Devices, Ministry of Education, School of Electronic Science and Engineering, Xi'an Jiaotong University, Xi'an 710049, China
[b] Institute of Spectroscopy, Russian Academy of Sciences, Troitsk 108840, Russia
[c] Moscow Institute of Physics and Technology (National Research University), Dolgoprudny 141701, Russia
[d] Skolkovo Institute of Science and Technology, Moscow, Territory of innovation center "Skolkovo", Moscow 121205, Russia
[e] Quantum Technology Centre, Faculty of Physics, M. V. Lomonosov Moscow State University, Moscow 119991, Russia
[f] Faculty of Physics, Higher School of Economics, Moscow 105066, Russia

ARTICLE INFO

Article history:
Received 27 February 2026
Received in revised form 12 May 2026
Accepted 12 June 2026
Available online 30 June 2026

Keywords:
Fractal topological insulators
Corner states
Vortex beams
Topological states

ABSTRACT

Quantized vortices are ubiquitous in physics, spanning superconductivity, astrophysics, superfluid condensed matter systems, and nonlinear optics. Yet embedding vorticity into topologically protected nonlinear states has remained a major challenge, with all previously observed corner solitons in higher-order topological insulators (HOTIs) exhibiting only trivial phase distributions. Here, we report on the first realization of stable topological corner vortex solitons in a photonic fractal HOTI. Using an array of laser-written waveguides in the shape of Sierpiński gasket with a controllable distortion, we design linear topological vortex modes, from which nonlinear corner vortex solitons bifurcate. Moreover, we demonstrate that these solitons exhibit exceptional robustness across a broad power range and, unlike vortex solitons in topologically trivial lattices, form without a power threshold. Our results introduce the angular momentum degree of freedom into the physics of topological corner modes, opening prospects for topologically protected vortex-based photonics.

1. Introduction

Topological materials represent a fundamentally new phase of matter, characterized by a qualitatively distinct behavior of bulk and boundary excitations [1–4]. Although insulating in the bulk, these materials support the propagation of exceptionally robust in-gap excitations at their edges that are protected by the material's band topology. Such topological excitations can carry information and energy, enabling robust transmission along the edges of material even in the presence of defects, edge deformations or bends. These features align well with modern technologies of information encoding in the phase of propagating fields, including the use of topological charges of nested vortices. However, embedding the vorticity into topological states remains elusive. The properties and localization of topological states are intrinsically tied to the symmetry of the bulk [5] and edge geometry of the material. Since vortex-carrying states typically occupy multiple sites of the system, they are difficult to harmonize with the specific symmetry of topological edge states. Moreover, the nature of topological insulators imposes fundamental constraints on the dimensionality and spatial extent of the topological states that can emerge. For example, in conventional topological insulators, the effective dimensionality of the edge states is only one lower than that of the bulk, and they are extended in the direction along the edge [1–3]. Higher-order topological insulators (HOTIs) extend this paradigm by supporting corner-localized modes whose effective dimensionality is reduced by at least two relative to the bulk [6,7]. Thus, two-dimensional HOTIs [8–15] can host effectively zero-dimensional corner states.

As a universal physical phenomenon, HOTIs have been demonstrated across diverse platforms, including acoustics, photonics, matter-wave and optoelectronic systems [6,7]. Notably, HOTIs have been constructed not only in bulk-periodic structures [9–14,16–19], but also in aperiodic systems exhibiting discrete

* Corresponding authors.
E-mail addresses: zhangyiqi@xjtu.edu.cn (Y. Zhang), kartashov@isan.troitsk.ru (Y.V. Kartashov).

https://doi.org/10.1016/j.scib.2026.06.052
2095-9273/

rotational symmetry, with the most prominent examples being disclination structures [20–27] and fractals [28–33]. However, the creation of topological states with nontrivial phases like vortices is particularly challenging in HOTIs. Specifically, their excitations are strongly localized in the corners, their spectrum usually permits only single-mode states, and their properties are strongly dependent on geometry. As a consequence, only the simplest, single-mode corner states have been observed experimentally in HOTIs, while incorporation of vorticity into such modes remains a fundamental challenge. Meanwhile, the interplay of topology and nonlinearity has attracted intense interest, because nonlinear self-action enables families of self-sustained states that inherit topological protection from their linear counterparts [34–36]. In photonic systems, for example, nonlinearity serves as a versatile knob for control of localization, internal structure and evolution of topological states [37–41]. Despite theoretical proposals and experimental progress on nonlinear corner states in HOTIs [42–46] and in polaritonics [47–51], all corner solitons observed to date also have exhibited only trivial phase distributions, while self-sustained corner states carrying global vorticity have not been reported. This is connected with the fact that vortex solitons represent excited higher-order states of the system that are typically prone to azimuthal instabilities and that usually require considerable power thresholds for their formation, at least in topologically trivial systems.

Here we demonstrate experimentally stable topological corner vortex solitons in a photonic fractal HOTI realized as a Sierpiński-gasket array of fs-laser-written single-mode waveguides. Fractal HOTIs host multiple in-gap corner modes with tunable degeneracies, which enables the construction of linear corner vortex modes using a superposition of states from a degenerate corner doublet. Crucially, the emergence of such corner doublets stems from the fractal structure of the waveguide arrays and is independent of the discrete rotational symmetry of the entire Sierpiński-gasket array. To the best of our knowledge, such corner doublets are not found in conventional HOTIs that were widely analyzed previously and that are based on either square (Su-Schrieffer-Heeger-like) or honeycomb lattices [6]. The spectra of these systems either lack degenerate corner states entirely, or when they do exist, linear combinations of such states do not lead to vortices near the corners of the structure. We show that self-focusing nonlinearity generates continuous families of corner vortex solitons that bifurcate from an in-gap vortex eigenstate, explaining their thresholdless formation in the topological regime. Since the localization of such states strongly depends on their position within the topological gap, nonlinearity enables precise tuning of the shapes of corner vortex solitons, thereby introducing a desired control into this topological platform. We confirm vorticity directly via phase-resolved interferometry, revealing a persistent phase singularity between the three corner waveguides for $m = \pm 1$.

2. Theoretical modeling

Propagation of light in waveguide arrays considered here is governed by the dimensionless nonlinear Schrödinger equation for light field amplitude ψ

$$\mathrm{i}\frac{\partial\psi}{\partial z} = -\frac{1}{2}\nabla^2\psi - \mathscr{R}(x,y)\psi - |\psi|^2\psi, \tag{1}$$

where (x, y) and z are the transverse coordinates and propagation distance, respectively; $\nabla^2 \equiv \partial_x^2 + \partial_y^2$; the function

$$\mathscr{R}(x,y) = p\sum_{m,n}\exp\left(-\frac{(x-x_{m,n})^2}{w_x^2} - \frac{(y-y_{m,n})^2}{w_y^2}\right)$$

describes waveguide array composed from waveguides of depth p, widths w_x, w_y, with centers in $(x_{m,n}, y_{m,n})$ points. Stationary solutions of Eq. (1) have the form $\psi = u(x,y)\mathrm{e}^{\mathrm{i}bz}$ and can be obtained from the equation

$$bu = \frac{1}{2}\nabla^2 u + \mathscr{R}(x,y)u + |u|^2 u,$$

where u describes the profile of the state and b is its propagation constant (eigenvalue).

To provide the mapping between dimensionless power U of light beams in numerical modeling, which is defined as

$$U = \iint |\psi|^2 \mathrm{d}x\mathrm{d}y \tag{2}$$

and real peak power P, we use standard normalizations adopted in our previous works [45,46], where the real field amplitude $\mathscr{E}$ and the dimensionless one are connected as

$$\mathscr{E} = \left(\frac{n}{k^2 r_0^2 n_2}\right)^{1/2}\psi, \tag{3}$$

where $k = 2\pi n/\lambda$ and $\lambda = 800\,\mathrm{nm}$ is the central working wavelength, while $r_0 = 10\,\mu\mathrm{m}$ is the characteristic spatial scale to which transverse coordinates x, y are normalized. The unperturbed refractive index of fused silica is $n = 1.45$. In this case, the relation between P and U is given by

$$P = \iint r_0^2|\mathscr{E}|^2\mathrm{d}x\mathrm{d}y = \frac{n}{k^2 n_2}\iint |\psi|^2\mathrm{d}x\mathrm{d}y = \frac{n}{k^2 n_2}U, \tag{4}$$

where the nonlinear coefficient $n_2 \approx 2.7\times 10^{-20}\,\mathrm{m}^2/\mathrm{W}$ at the wavelength $\lambda = 800\,\mathrm{nm}$ for fused silica.

3. Results

3.1. Lattice, spectrum, and modes

We consider third-generation (G_3) Sierpiński gasket fractal arrays created using fs-laser writing [52–54] as a structure for realization of HOTI. Schematic illustrations and microphotographs of the arrays are shown in Fig. 1a (see Section S1 in the Supplementary Materials). Self-similar fractal structures characterized by a non-integer effective dimensionality have been established as a perspective platform for investigation of topological phenomena [28–33,45,55,56]. These structures are aperiodic and sometimes considered as lacking a well-defined insulating bulk, while their topological characterization requires real-space invariants [29,30,55,56]. We introduce controllable Kekulé-like distortion (that is also known as Wu-Hu approach [57]) already into first-generation (G_1) arrays (see Fig. 1a), characterized by a shift r indicated in G_1, while keeping next-nearest spacing a fixed. The parameters of arrays entering into function $\mathscr{R}(x,y)$ describing refractive index distribution in such structures are indicated in the caption of Fig. 1.

Neglecting nonlinearity and using plane-wave expansion method, we obtain the linear spectrum of modes of the fractal array as a function of parameter r displayed in Fig. 1b (see also the dependencies of all eigenvalues b on mode index n for representative values of $r = 0.3a, 0.5a$ and $0.7a$ corresponding to dashed lines in $b(r)$ plot). The fractal HOTI hosts multiple in-gap topological modes (colored dots) associated with internal and external boundaries [33].

At $r < 0.5a$, a manifold of nearly degenerate states (green line in Fig. 1b) appears in the internal and external corners of the structure (Fig. 1c). At $r > 0.5a$, several coexisting topological states in outer corners appear. The orange line in Fig. 1b corresponds to

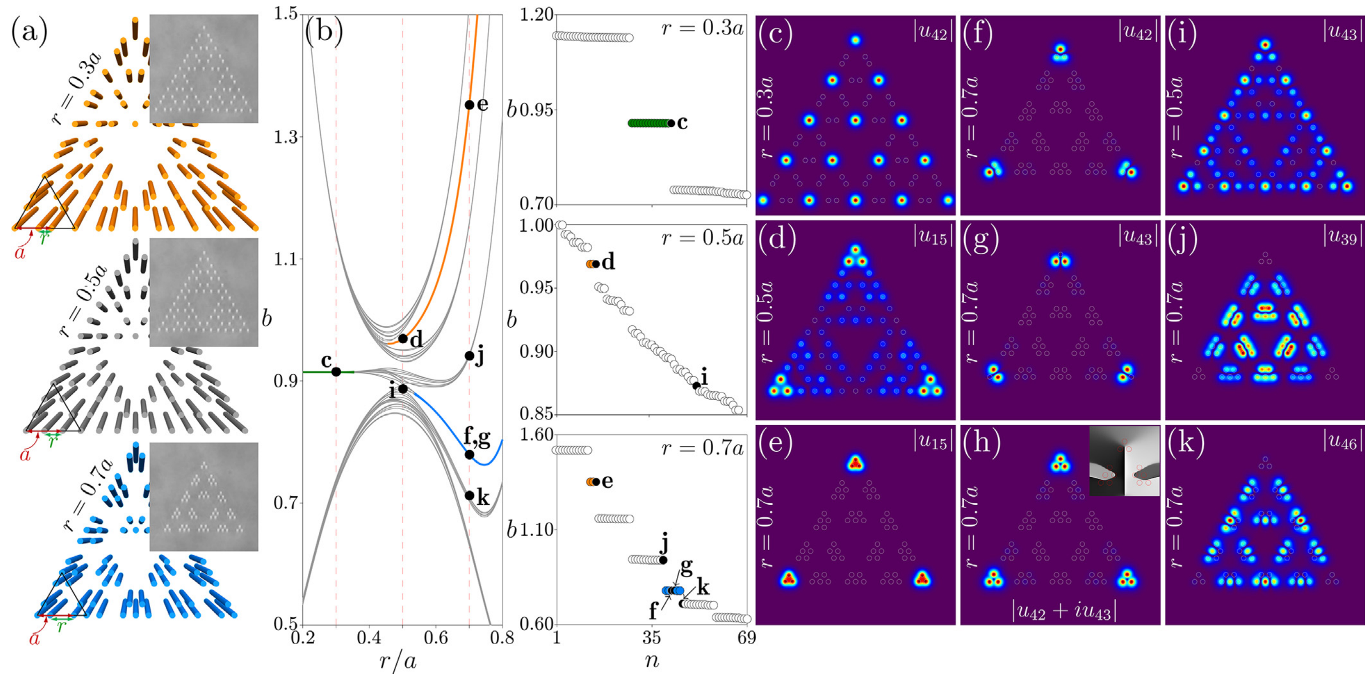

Fig. 1. Lattices, spectra, and modes. (a) Sketches of the fractal G_3 waveguide arrays with different distortion parameters r. Triangles indicate G_1 elements. The insets show microphotographs of corresponding fs-laser written arrays. (b) Linear spectrum of G_3 fractal array as a function of r and eigenvalues b vs mode index n corresponding to three vertical dashed lines in (b). Colored dots correspond to topological states, gray dots to delocalized states. Black dots with letters correspond to representative eigenmodes u_n, whose $|u_n|$ distributions (with superimposed on them array contours) are depicted in panels (c–k). Among them are two degenerate corner states u_{42} (f) and u_{43} (g) that can be used to construct corner vortex state $u_{42}+iu_{43}$ whose modulus and phase are shown in (h). Panels in (c–k) are shown in $-25 \leqslant x, y \leqslant 25$. Array parameters are $a = 3.4, w_x = 0.8, w_y = 0.85$, and $p = 3.3$.

threefold degenerate states (mode index n = 13–15), where three corner spots are in-phase (Fig. 1d and e). Their localization increases when one moves away from $r = 0.5a$ point corresponding to equal waveguide spacing. Of particular interest is the blue branch at $r > 0.5a$ which corresponds to sixfold degenerate modes (index n = 40–45) and contains pairs with different structures of spots in array corners (see exemplary states u_{42} and u_{43} in Fig. 1f and g). Their superposition $u_{42} + iu_{43}$ forms a linear corner vortex state (Fig. 1h). The phase singularity in such states is positioned between three corner waveguides (inset in Fig. 1h), and the mode's localization increases with the shift parameter r. We stress that the appearance of pairs of degenerate modes residing in the same corner is unique for selected fractals and is not tied to discrete rotational symmetry $\mathscr{C}_3$ of the entire structure (the symmetry axis passes through the center of the array, but not near its corners). At the same time, if one considers three corner waveguides as an isolated subsystem from the rest of the lattice, it would also have discrete rotational symmetry $\mathscr{C}_3$. In accordance with group theory arguments [58], such systems can support vortex modes with topological charges not exceeding $m = 1$. The examples of delocalized states (associated with gray lines in Fig. 1b) coexisting with topological ones are shown in Fig. 1i–k. Notice that topological nature of modes from colored branches in Fig. 1b is confirmed by nonzero values of real-space polarization index for them, as discussed in Refs. [29–31,45].

3.2. Families of corner vortex solitons

In a nonlinear medium, topological corner vortex states give rise to families of corner vortex solitons that can be obtained by the Newton method. They are characterized by power $U = \iint |\psi|^2 dxdy$ shown in Fig. 2a as a function of propagation constant b. We emphasize that corner vortex solitons bifurcate from linear vortex states (see blue curve, where $U \to 0$ when b approaches eigenvalue of linear vortex at a given r) and exist across several spectral gaps. This is the key mechanism underlying thresholdless formation: the nonlinear state emerges continuously from an already localized in-gap vortex eigenstate rather than requiring finite-power self-trapping. When b enters into the band of delocalized states, coupling with them occurs, resulting in delocalization of corner state and rapid increase of power U (compare soliton profiles in Fig. 2b and c from the same family). Nevertheless, the continuation of the family of vortex solitons can also be obtained in higher-lying gaps (orange and green curves) that, in turn, couple with delocalized states when power becomes too high (compare profiles in Fig. 2d and e). Thus, one can consider that while the bands of delocalized states locally "interrupt" the continuity of the corner vortex soliton families, all such corner vortex soliton families marked by different colors in distinct band gaps do originate from corresponding linear corner states. One can also conclude that nonlinearity introduces tunability in our system and allows for considerable reshaping of self-sustained states even in fabricated structures with a fixed r/a parameter.

The variation of shapes of corner vortex solitons with increase of power strongly depends on chosen value of distortion parameter r. Thus, when r is closer to $0.5a$, linear corner vortex states appear much less localized and extend into the array. In this case, when one increases the propagation constant b (and hence the peak power of solution U), corner solitons originating from such moderately localized linear corner modes do experience visible reshaping already in the gap — their localization initially increases with increase of b. When the propagation constant of such solitons crosses the band of delocalized states, they also exhibit delocalization. In this case, one observes nonmonotonic variation of soliton width with increase of b, as shown in Section S4 in the Supplementary Materials.

We stress that corner vortex solitons in fractals are stable in a broad range of powers, as confirmed by their propagation with added noise (up to 5% in amplitude) in the frames of Eq. (1) over

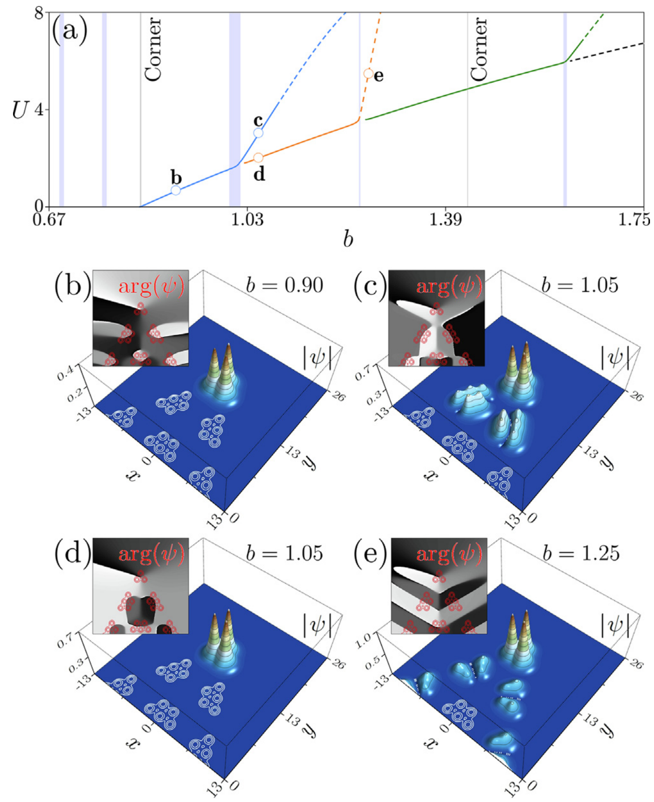

Fig. 2. Corner vortex soliton family. (a) Power U of corner vortex solitons in a fractal array as a function of b at $r = 0.7a$. Solid (dashed) lines correspond to stable (unstable) solitons. Purple regions indicate bands of extended states, while gray lines show eigenvalues of linear corner states. (b)–(e) Field modulus and phase (insets) distributions in solitons corresponding to the dots with letters in (a).

a huge distance $z \sim 4000$, far exceeding sample length. Stable branches in Fig. 2a are shown with solid lines, unstable ones with dashed lines. Notice stability in finite gaps, and instability in a semi-infinite gap (see Section S3 in the Supplementary Materials, where we also present the details of linear stability analysis).

3.3. Observation of corner vortex solitons

To realize corner vortex solitons, we used fractal waveguide arrays inscribed in fused silica (unperturbed refractive index $n = 1.45$ and nonlinear coefficient $n_2 \approx 2.7 \times 10^{-20}\,\mathrm{m^2/W}$ at the wavelength $\lambda = 800\,\mathrm{nm}$) with next-nearest waveguide spacing of $34\,\mu\mathrm{m}$ (corresponding to $a = 3.4$) and various shift parameters r from $0.4a$ to $0.8a$. The 99.1 mm physical sample length corresponds to $z \approx 87$ in our theoretical model (characteristic diffraction length of 1.14 mm is used in normalization of z for beam width of 10 μm). The evaluated refractive index modulation depth in array $\delta n \sim 3.7 \times 10^{-4}$ corresponds to $p = 3.3$ adopted in simulations. The implemented "multi-scan" writing technology (see Section S2 in the Supplementary Materials) allows the creation of waveguides supporting nearly circular modes (even though the cross-sections of such waveguides in microphotographs in Fig. 1a may look slightly rectangular). This results in a nearly isotropic coupling between the waveguides. In simulations, the couplings in such a system are accurately captured by considering just minimal ellipticity of waveguides: $w_x = 0.8$ and $w_y = 0.85$. Namely, such minimal ellipticity guarantees that modes giving rise to corner vortex states remain practically degenerate in a broad interval of distortion parameters r, see Fig. 1b. To efficiently excite corner vortex solitons, we used a spatially structured pulsed laser excitation (580 fs pulses of variable energy E obtained from 1 kHz Ti:sapphire laser system, which provides high peak powers P up to several MW). Using the reflective spatial light modulator (SLM), we created a three-spot pattern with properly designed phases $2\pi m(\kappa - 1)/3$, where $m = \pm 1$ is the topological charge, and $\kappa = 1, 2, 3$ is the index of corresponding laser beams. The beams of equal intensities with desired phases are then focused onto three corner waveguides. We note that the implemented structured excitation ensures a strong overlap with the desired corner vortex state (see Section S2 in the Supplementary Materials for details).

To illustrate the importance of the shift parameter r for emergence of topological corner states, we first consider the array with $r = 0.5a$, where all eigenmodes of the array are effectively extended. Using three-spot input with in-phase spots (that corresponds to $m = 0$) focused into three corner waveguides reveals strong diffraction broadening at low peak powers $P \sim 0.01$ MW (see Fig. 3a showing corresponding experimental output intensity distributions with maroon background). Only with an increase of input peak power to values $P > 2$ MW, one observes the contraction of light to three corner waveguides and formation of a compact corner soliton that in this case occurs above a considerable power threshold. Notice that for $m = 0$ input, the output pattern is symmetric with respect to $x = 0$ axis. These observations are confirmed by theoretically calculated output intensity distributions at different dimensionless powers U shown in Fig. 3b (images with purple background). Using vortex-carrying inputs with $m = +1$ (Fig. 3c) and $m = -1$ (Fig. 3d) reveals stronger diffraction for the same peak low and moderate power levels P that becomes notably asymmetric. The formation of a corner vortex soliton occurs in this case above an even higher power threshold $P \sim 3$ MW. We observed similar outputs in arrays with $r = 0.4a$.

Experimental evidence of thresholdless topological corner vortex solitons is presented in Fig. 4 in a fractal array with shift parameter $r = 0.7a$ that supports well-localized linear corner vortex states. When using three-spot input with $m = -1$ vortex, we observed (Fig. 4a) that light remains confined predominantly in three corner waveguides across all power levels, from $P = 0.01$ MW to $P = 3$ MW (limited by the material damage threshold), and that vortical phase structure, with a singularity between three corner waveguides, is present in all cases. This confirms thresholdless and topological nature of such solitons (i.e., their bifurcation from in-gap linear vortex corner states), as well

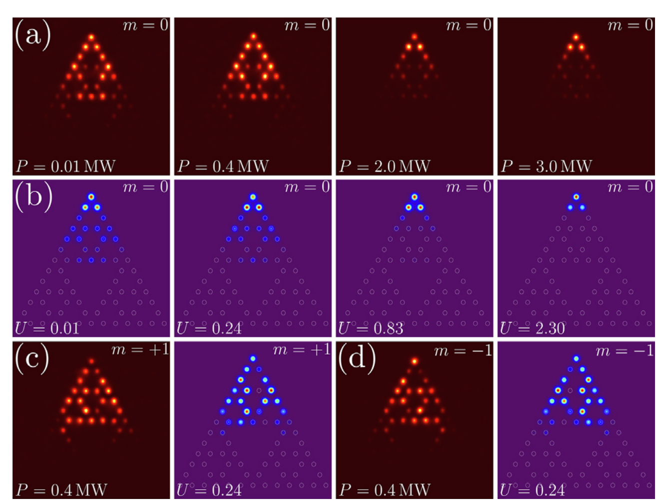

Fig. 3. Experimental excitations in topologically trivial lattice. (a) Output experimental intensity distributions (panels with maroon background) for trivial-phase excitation ($m = 0$) of three corner waveguides in a fractal array with $r = 0.5a$ at different input peak powers P compared with (b) theoretical output distributions (panels with purple background). (c) and (d) show comparison of the experimental and theoretical output intensity distributions for vortex-carrying excitation of three corner waveguides with $m = +1$ (c) and $m = -1$ (d).

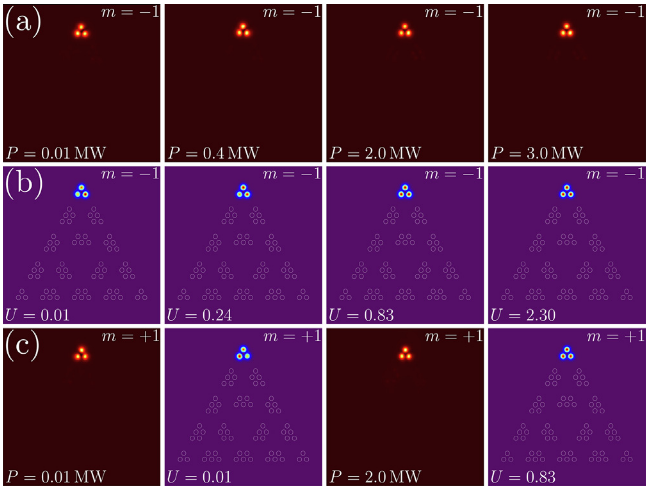

Fig. 4. Experimental excitation of corner vortex solitons. Comparison of experimental (a) and theoretical (b) output intensity distributions for vortex-carrying excitation ($m = -1$) of three corner waveguides in an array with $r = 0.7a$ at different peak powers. (c) The same for $m = +1$ excitation.

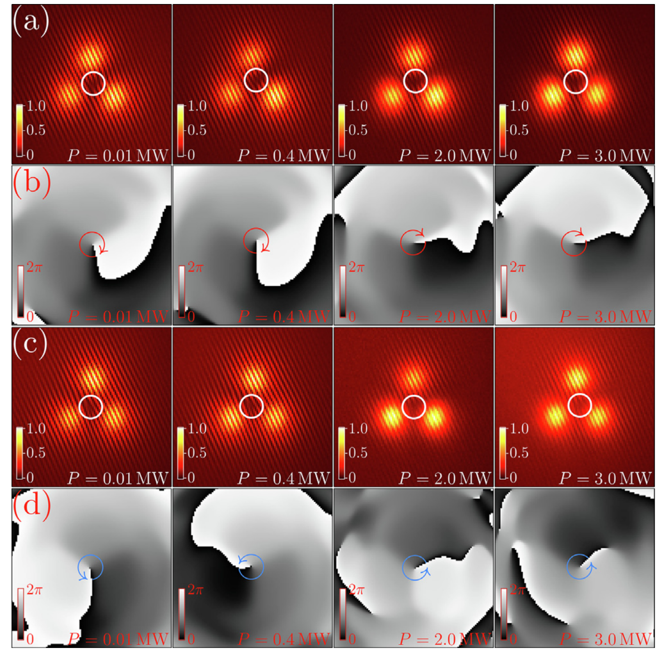

Fig. 5. Experimentally measured phase distribution of the excited corner vortex soliton. (a, c) Experimentally measured single-shot interference patterns and corresponding retrieved phase distributions (b, d). Measured phases confirm the formation of corner vortex solitons with topological charge $m = -1$ (a, b) and $m = +1$ (c, d) at different peak powers P. White circles schematically denote the position of the phase singularity.

as their exceptional robustness. Notice that output intensity distributions are slightly distorted at low and moderate peak powers (i.e., they do not feature ideal $\mathscr{C}_3$ discrete rotational symmetry). This is a consequence of slight ellipticity of waveguide modes that cannot be eliminated completely even with "multi-scan" writing technique. Increasing peak power to $P = 2$ MW practically eliminates this distortion. These observations are in agreement with theoretical simulations shown in Fig. 4b. Similar results for $m = +1$ vortex-carrying inputs (Fig. 4c) confirm the system's high symmetry.

As one can see from theoretical plots in Fig. 2, coupling with extended states in the band should result in the appearance of long tails inside the array. We do not see such tails (that would clearly indicate nonlinearity-induced reshaping) in experiments, only because for chosen distortion parameter r value they start to appear for peak powers $P > 3$ MW that is close to the material damage threshold. For this reason, to avoid sample damage, we did not increase peak power well above 3 MW. At the same time, by looking at distributions in Fig. 3 (in the trivial case), one can see that the nonlinear contribution to the refractive index is considerable at such peak powers and notably changes output intensity distributions, so this regime is indeed strongly nonlinear.

To unequivocally confirm the vortical structure of the output fields in Fig. 4, we recorded and analyzed single-shot interference patterns of output fields with a coherent plane wave for different peak powers to retrieve the output phase distributions (see Section S1 in the Supplementary Materials). Experimentally measured normalized fringe patterns and corresponding phase distributions, zoomed in around three corner waveguides, are shown in Fig. 5a and b for $m = -1$ and in Fig. 5c and d for $m = +1$ vortex solitons, respectively. The fork (denoted with white circles) in the interference pattern with orientation reflecting the charge of the vortex is present between the corner waveguides at all peak power levels. Retrieved phases conclusively confirm global vorticity imposed on the field for both $m = -1$ and $m = +1$ cases.

4. Conclusion

Summarizing, we have experimentally observed corner vortex solitons in nonlinear HOTIs based on a fractal waveguide array and verified their vorticity by phase-resolved interferometry. The essential mechanism is the degeneracy-enabled construction of an in-gap corner vortex eigenstate, which yields thresholdless nonlinear continuation into robust vortex-soliton families. We found that observed vortex solitons in fractal arrays are exceptionally robust in a broad power range and that localization of the vortex-carrying modes can be changed via design of the underlying fractal structure. Our work opens a route to the investigation of diverse nonlinear phenomena in topologically nontrivial systems hosting vortices. This includes generation of new frequencies and states with higher topological charges, nonlinearity-controlled switching, and lasing.

Our findings reveal a rich interplay among fractality, topology, orbital angular momentum degree of freedom, and nonlinearity. They open avenues for experimental studies of fractal topological systems in domains beyond photonics, such as acoustics and matter-wave physics. While obtained for self-focusing nonlinearity, our results can be generalized to the case of self-defocusing materials. Furthermore, instead of the waveguide array systems, topological fractal micropillar arrays could be realized in exciton–polariton microcavities or other dissipative/-cavity platforms [59]. Under resonant pumping [60], such systems may support lasing in corner vortex solitons and exhibit bistability effects with vortices. The system proposed here could be generalized to nanoscale settings, to achieve the formation of topologically protected nano-vortices, by analogy with recent experiments with lasing on topological disclinations [26]. Finally, vortex-carrying states and new aspects of their localization associated with fractality of topological structure could be explored in p-orbital HOTIs [61,62].

Conflict of interest

The authors declare that they have no conflict of interest.

Acknowledgments

This work was supported by the Natural Science Basic Research Program of Shaanxi Province (2024JC-JCQN-06, 2025JC-QYCX-006), the National Natural Science Foundation of China (12474337), the Key Research and Development Program of Shaanxi Province (2025CY-YBXM-037), the Postdoctoral Research Project of Shaanxi Province (2023BSHYDZZ14), the Sichuan Science and Technology Program (2025ZNSFSC1458), the Russian Science Foundation (grant 24–12-00167) and partially by the project FFUU-2024–0003 of the Institute of Spectroscopy of RAS.

Author contributions

Yiqi Zhang and Yaroslav V. Kartashov conceived the idea, provided theoretical analysis and numerical simulations, and supervised the project. Yongdong Li, Pavlos G. Lagoudakis, Sergei P. Kulik, and Victor N. Zadkov co-supervised the project. Alexander V. Kireev, Khalil Sabour, Victor O. Kompanets, Sergey Y. Alyatkin, and Sergey V. Chekalin conducted the experiment. Nikita S. Kostyuchenko, Sergei A. Zhuravitskii, Nikolay N. Skryabin, and Alexander A. Kalinkin fabricated the samples. All authors contributed to interpretation of experimental results and writing of the paper.

Appendix A. Supplementary material

Supplementary data to this article can be found online at https://doi.org/10.1016/j.scib.2026.06.052.

References

[1] Lu L, Joannopoulos JD, Soljačić M. Topological photonics. Nat Photon 2014;8:821–9.
[2] Ozawa T, Price HM, Amo A, et al. Topological photonics. Rev Mod Phys 2019;91:015006.
[3] Zhang X, Zangeneh-Nejad F, Chen ZG, et al. A second wave of topological phenomena in photonics and acoustics. Nature 2023;618:687–97.
[4] Leykam D, Xue H, Zhang B, et al. Limitations and possibilities of topological photonics. Nat Rev Phys 2026;8:55–64.
[5] Wieder BJ, Bradlyn B, Cano J, et al. Topological materials discovery from crystal symmetry. Nat Rev Mater 2022;7:196–216.
[6] Xie B, Wang HX, Zhang X, et al. Higher-order band topology. Nat Rev Phys 2021;3:520–32.
[7] Lin ZK, Wang Q, Liu Y, et al. Topological phenomena at defects in acoustic, photonic and solid-state lattices. Nat Rev Phys 2023;5:483–95.
[8] Benalcazar WA, Bernevig BA, Hughes TL. Quantized electric multipole insulators. Science 2017;357:61–6.
[9] Serra-Garcia M, Peri V, Süsstrunk R, et al. Observation of a phononic quadrupole topological insulator. Nature 2018;555:342–5.
[10] Noh J, Benalcazar WA, Huang S, et al. Topological protection of photonic mid-gap defect modes. Nat Photon 2018;12:408–15.
[11] Xie BY, Su GX, Wang HF, et al. Visualization of higher-order topological insulating phases in two-dimensional dielectric photonic crystals. Phys Rev Lett 2019;122:233903.
[12] Chen XD, Deng WM, Shi FL, et al. Direct observation of corner states in second-order topological photonic crystal slabs. Phys Rev Lett 2019;122:233902.
[13] El Hassan A, Kunst FK, Moritz A, et al. Corner states of light in photonic waveguides. Nat Photon 2019;13:697–700.
[14] Li M, Zhirihin D, Gorlach M, et al. Higher-order topological states in photonic kagome crystals with long-range interactions. Nat Photon 2020;14:89–94.
[15] Benalcazar WA, Cerjan A. Chiral-symmetric higher-order topological phases of matter. Phys Rev Lett 2022;128:127601.
[16] Peterson CW, Benalcazar WA, Hughes TL, et al. A quantized microwave quadrupole insulator with topologically protected corner states. Nature 2018;555:346–50.
[17] Mittal S, Orre VV, Zhu G, et al. Photonic quadrupole topological phases. Nat Photon 2019;13:692–6.
[18] Zhang X, Wang HX, Lin ZK, et al. Second-order topology and multidimensional topological transitions in sonic crystals. Nat Phys 2019;15:582–8.
[19] Peterson CW, Li T, Benalcazar WA, et al. A fractional corner anomaly reveals higher-order topology. Science 2020;368:1114–8.
[20] Peterson CW, Li T, Jiang W, et al. Trapped fractional charges at bulk defects in topological insulators. Nature 2021;589:376–80.
[21] Liu Y, Leung S, Li FF, et al. Bulk-disclination correspondence in topological crystalline insulators. Nature 2021;589:381–5.
[22] Li T, Zhu P, Benalcazar WA, et al. Fractional disclination charge in two-dimensional C_n-symmetric topological crystalline insulators. Phys Rev B 2020;101:115115.
[23] Wang Q, Ge Y, Sun Hx, et al. Vortex states in an acoustic Weyl crystal with a topological lattice defect. Nat Commun 2021;12:3654.
[24] Ren B, Wang H, Kartashov YV, et al. Nonlinear photonic disclination states. APL Photon 2023;8:016101.
[25] Ren B, Arkhipova AA, Zhang Y, et al. Observation of nonlinear disclination states. Light Sci Appl 2023;12:194.
[26] Hwang MS, Kim HR, Kim J, et al. Vortex nanolaser based on a photonic disclination cavity. Nat Photon 2024;18:286–93.
[27] Huang C, Shang C, Kartashov YV, et al. Vortex solitons in topological disclination lattices. Nanophoton 2024;13:3495–502.
[28] Manna S, Nandy S, Roy B. Higher-order topological phases on fractal lattices. Phys Rev B 2022;105:L201301.
[29] Li J, Mo Q, Jiang JH, et al. Higher-order topological phase in an acoustic fractal lattice. Sci Bull 2022;67:2040–4.
[30] Zheng S, Man X, Kong ZL, et al. Observation of fractal higher-order topological states in acoustic metamaterials. Sci Bull 2022;67:2069–75.
[31] Ren B, Kartashov YV, Maczewsky LJ, et al. Theory of nonlinear corner states in photonic fractal lattices. Nanophoton 2023;12:3829–38.
[32] Li M, Li C, Yan L, et al. Fractal photonic anomalous Floquet topological insulators to generate multiple quantum chiral edge states. Light Sci Appl 2023;12:262.
[33] Eek L, Osseweijer ZF, Morais Smith C. Fractality-induced topology. Phys Rev Lett 2025;134:246601.
[34] Kartashov YV, Arkhipova AA, Zhuravitskii SA, et al. Observation of edge solitons in topological trimer arrays. Phys Rev Lett 2022;128:093901.
[35] Chen R, Yan W, Liu W, et al. Nonlinear tuning of multiple topological edge states in photovoltaic photonic lattices. Sci Bull 2025;70:1605–10.
[36] Du H, Zhao H, Li Y, et al. Observation of nonlinear edge states in an interacting atomic trimer array. Light Sci Appl 2025;14:296.
[37] Smirnova D, Leykam D, Chong Y, et al. Nonlinear topological photonics. Appl Phys Rev 2020;7:021306.
[38] Szameit A, Rechtsman MC. Discrete nonlinear topological photonics. Nat Phys 2024;20:905–12.
[39] Maczewsky LJ, Heinrich M, Kremer M, et al. Nonlinearity-induced photonic topological insulator. Science 2020;370:701–4.
[40] Mukherjee S, Rechtsman MC. Observation of Floquet solitons in a topological bandgap. Science 2020;368:856–9.
[41] Sone K, Ezawa M, Ashida Y, et al. Nonlinearity-induced topological phase transition characterized by the nonlinear Chern number. Nat Phys 2024;20:1164–70.
[42] Kirsch MS, Zhang Y, Kremer M, et al. Nonlinear second-order photonic topological insulators. Nat Phys 2021;17:995–1000.
[43] Hu Z, Bongiovanni D, Jukić D, et al. Nonlinear control of photonic higher-order topological bound states in the continuum. Light Sci Appl 2021;10:164.
[44] Ezawa M. Nonlinearity-induced transition in the nonlinear Su-Schrieffer-Heeger model and a nonlinear higher-order topological system. Phys Rev B 2021;104:235420.
[45] Zhong H, Kompanets VO, Zhang Y, et al. Observation of nonlinear fractal higher order topological insulator. Light Sci Appl 2024;13:264.
[46] Kompanets VO, Feng S, Zhang Y, et al. Observation of nonlinear topological corner states originating from different spectral charges. Adv Mater 2025;37:2500556.
[47] Banerjee R, Mandal S, Liew TCH. Coupling between exciton-polariton corner modes through edge states. Phys Rev Lett 2020;124:063901.
[48] Zhang Y, Kartashov YV, Torner L, et al. Nonlinear higher-order polariton topological insulator. Opt Lett 2020;45:4710–3.
[49] Wu J, Ghosh S, Gan Y, et al. Higher-order topological polariton corner state lasing. Sci Adv 2023;9:eadg4322.
[50] Schneider T, Gao W, Zentgraf T, et al. Topological edge and corner states in coupled wave lattices in nonlinear polariton condensates. Nanophoton 2024;13:509–18.
[51] Bennenhei C, Shan H, Struve M, et al. Organic room-temperature polariton condensate in a higher-order topological lattice. ACS Photon 2024;11:3046–54.
[52] Szameit A, Nolte S. Discrete optics in femtosecond-laser-written photonic structures. J Phys B: At Mol Opt Phys 2010;43:163001.
[53] Skryabin NN, Zhuravitskii SA, Dyakonov IV, et al. Femtosecond-laser-written low-loss multiscan waveguides in fused silica. Phys Rev Appl 2024;22:064079.
[54] Yan W, Zhang B, Chen F. Photonic topological insulators in femtosecond laser direct-written waveguides. npj Nanophoton 2024;1:40.
[55] Yang Z, Lustig E, Lumer Y, et al. Photonic Floquet topological insulators in a fractal lattice. Light Sci Appl 2020;9:128.
[56] Biesenthal T, Maczewsky LJ, Yang Z, et al. Fractal photonic topological insulators. Science 2022;376:1114–9.
[57] Wu LH, Hu X. Scheme for achieving a topological photonic crystal by using dielectric material. Phys Rev Lett 2015;114:223901.
[58] Ferrando A, Zacarés M, García-March MA. Vorticity cutoff in nonlinear photonic crystals. Phys Rev Lett 2005;95:043901.
[59] Klembt S, Harder TH, Egorov OA, et al. Exciton-polariton topological insulator. Nature 2018;562:552–6.
[60] Kartashov YV, Skryabin DV. Bistable topological insulator with exciton-polaritons. Phys Rev Lett 2017;119:253904.
[61] Zhang Y, Bongiovanni D, Wang Z, et al. Realization of photonic p-orbital higher-order topological insulators. eLight 2023;3:5.
[62] Bongiovanni D, Hu Z, Wang Z, et al. p-orbital higher-order topological corner states in 2D photonic Su-Schrieffer-Heeger lattices. Laser Photon Rev 2024;18:2400638.